Structure of high-stage potassium-intercalated graphite

Michael E. Huster,* Paul A. Heiney, and Victoria B. Cajipe
Department of Physics and Laboratory for Research on the Structure of Matter, University of Pennsylvania, Philadelphia, Pennsylvania 19104

John E. Fischer
Department of Materials Science and Engineering and Laboratory for Research on the Structure of Matter, University of Pennsylvania, Philadelphia, Pennsylvania 19104

(Received 11 August 1986)

We have used x-ray diffraction to study the structure of stage-4 through stage-11 potassium-intercalated graphite as a function of temperature. The (00.L) diffraction patterns are analyzed in terms of the Hendricks-Teller model for a disordered one-dimensional crystal. Stage 4—5 samples are best described by phase separation of two different stages, while higher-stage samples are best described by a broad distribution of *many* stages. In plane, all samples show a high-temperature two-dimensional fluid structure of the potassium atoms. In the stage 4—6 samples, the fluid peak gradually sharpens on cooling and increases in intensity to form a two-dimensional incommensurate superlattice. This evolution is consistent with a second-order transition. By contrast, the higher-stage samples show a strongly first order, hysteretic transition to a commensurate $\sqrt{7}\times\sqrt{7}$ superlattice at 235 K. In all cases, the expansion of the two-dimensional lattice upon freezing agrees within experimental error with the 2—4 % increase in out-of-plane density of potassium layers.

I. INTRODUCTION

The last decade has seen intense research in the structural and electronic properties of graphite intercalation compounds.[1–5] This interest is due in part to the lower-dimensional character of these materials. The phenomenon of staging, in which intercalant atoms fill some galleries and not others in a periodic fashion, is essentially one dimensional, while the ordering of intercalant atoms within each layer can be either three-dimensional or quasi-two-dimensional (2D). The effective dimensionality of each system depends on the type of transition, the intercalant, and the stage of the sample. Potassium-intercalated-graphite (K-Gr) has been widely studied, in part because of its simplicity and ease of preparation, and because the interactions are well understood.[6]

From a structural point of view, the in-plane structure of intercalation compounds, the degree of stage disorder, and the relationship between in-plane and out-of-plane structure are all subjects of current research. Possibilities for the in-plane structure of high-temperature, disordered intercalant phases include true "lattice gasses," with intercalate atoms sitting in the centers of Gr hexagons, liquids with intercalate atoms moving freely through the host galleries, and a variety of intermediate structures, all of which have short-range order. The weakness of the diffracted signal generally precludes a detailed determination of the fluid structure, however, the in-plane density can be deduced from the position of the first fluid diffraction maximum. Recent work by Nishitani *et al.*,[7] conducted *in situ* at 600 K, has shown that the peak position of K-Gr, and thus the in-plane density, is not a constant for a given stage, but rather depends on the K chemical potential. Also, at room temperature or below, there are systematic variations in in-plane peak position versus stage, with higher stage compounds containing less dense in-plane fluids.

At low temperatures, the K atoms form ordered structures within the Gr galleries. The freezing-transition temperatures and the lowest in-plane peak positions are shown in Table I. At room temperature the K in the stage-one compound, KC_8, is ordered into a three-dimensional solid,[7,8] with a commensurate $2\times2R\,0°$ superlattice in-plane and $\alpha\beta\gamma\delta$ stacking along the c axis. At high temperature the superlattice metals into an in-plane

TABLE I. Positions of lowest in-plane peaks in disordered and solid phase, melting transition temperatures, and in-plane solid structure versus stage. IC denotes an incommensurate structure.

Stage	Q_{liq} (Å^{-1})	Q_{sol} (Å^{-1})	T_m (K)	Solid structure	References
1	1.45—1.34	1.47	700	$2\times2R\,0°$	7
2	1.23→1.178	1.20	125	IC	7,10,12,21,24
3—4	1.178→1.15	1.17→1.13	200	IC	11
5—7	1.13	1.11	235	$\sqrt{7}\times\sqrt{7}R\,19.1°$	42,43

fluid;[7] at room temperature and high pressure the in-plane structure becomes $\sqrt{3}\times\sqrt{3}R\,30°$.[9] Stages 2 through 4 are incommensurate in-plane[7-12] at all temperatures. There has been considerable speculation about the detailed nature of these structures.[2,11,13-19] Models include static distortion waves in an almost commensurate intercalant lattice,[13,14] periodic distortions of the Gr host,[11,15] a rotated, incommensurate lattice in which the atoms relax into the centers of the nearest Gr hexagons,[16] and a lattice of disclinations in a commensurate $\sqrt{7}\times\sqrt{7}R\,19°$ (Refs. 2, 17, and 18) or $9\times9R\,0°$ (Ref. 19) lattice. In general, the diffraction from such phases consists of Bragg peaks from the pure Gr host, Bragg peaks from an ideal unmodulated incommensurate lattice, and all sums and differences of these vectors; to distinguish between the various models requires a careful study of the intensities and positions of all these peaks. Stage-2 K-Gr orders at around 125 K into a 3D superlattice which is incommensurate with the graphitic planes and which is highly faulted along the c axis. This appears to be either a continuous transition or a smeared first-order transition. Then, at 95 K there is a first-order transition to a structure which has fewer stacking defects out of plane.[10] The stage-3 compound has a broad ordering transition at 190 K to an in-plane incommensurate solid, and a second broad ordering transition at 130 K in which three-dimensional correlations appear. In this paper we investigate the in-plane structure for stages 4 and above.

Since staging is seen in intercalation compounds with very different in-plane structures, and in many cases the stage is unchanged while the in-plane structure goes through a structural transition, a one-dimensional model can be used to describe staging in intercalation compounds. The first such model, due to Safran,[20] has repulsive Coulomb interactions between filled galleries, and an attractive interaction (due to elastic deformation of the graphite lattice) between intercalants within a gallery. The Hamiltonian employed is

$$H=-\mu\sum\sigma_i-\tfrac{1}{2}U_0\sum\sigma_i^2+\tfrac{1}{2}\sum V_{ij}\sigma_i\sigma_j\ ,$$

where μ is the chemical potential, σ_i are the layer occupancies, U_0 is the averaged in-plane attraction, and V_{ij} is the repulsive interplanar interaction. Since the intercalants usually reside at preferred sites, the in-plane structure has been modeled as a lattice gas with attractive interactions. A mean-field approximation then gives a form for the in-plane energy contribution as given above in the U_0 term. Based on band-structure calculations,[21] Safran takes

$$V_{ij}=\tfrac{1}{2}V\,|\,z\,|^{-\alpha}\ .$$

The phase diagram calculated by searching for periodic solutions to this model shows a high temperature transition to stage 1 for all intercalant densities. Since high-stage structures are entropically less stable there is a tendency for higher stages to disorder at progressively lower temperatures. There is a relatively narrow range of densities allowed for each pure stage; coexistence regions separate neighboring phases.

Although the Safran model reproduces the overall features of the experimental phase diagrams, it has several deficiencies. First, in addition to integer staging structures, this model predicts "fractional stages," in which there is more than one filled gallery per repeat distance. Indeed, it was shown by Bak and Bruinsma,[22] that the complete devil's staircase of staging structures exists for this model. With one exception[23] these fractional stages have not been observed experimentally. Secondly, the Safran model is symmetric in density about stage 2, while the experimental phase diagram of LiC_x measured by Woo *et al.*[24] is skewed towards low concentration. (The stage 2 of Woo *et al.* is also stable to a much higher temperature than Safran's model predicts.) Finally, the entropy of stage disorder is not included in this model.

Several other calculations[25-31] have used modified forms of Safran's Hamiltonian. For example, fractional stages are eliminated by strong screening of the out-of-plane interactions.[25] Likewise, the in-plane commensuration energy and the possibility of more than one in-plane structure can have an important effect on the staging structure.[31] The entropy of stage disorder is most significant at high temperature and high stage. Assuming finite-sized domains parallel to the planes of the host material, Kirczenow[30] finds that at high stage or high temperature, several randomly mixed stages may be present. At low temperatures pure stages are found, with narrow coexistence regions, in agreement with experiment. As the chemical potential decreases, the average stage increases, and the phases become less pure, consisting of mixtures of three or more stages. Thus, a sample prepared with a stoichiometry intermediate between stage 1 and stage 2 would be expected to phase separate into almost pure stage 1 and stage 2 regions; we might refer to a sample that was 70% stage 1 and 30% stage 2 by composition as being nominal stage 1.3, with the understanding that actual phase separation was implied. By contrast, a sample with nominal stage 10.3 would be expected to consist of a distribution of many package types such that the average package contains 10.3 carbon layers. The highest stage for which pure staging exists decreases with both increasing temperature and decreasing in-plane domain size. Computer simulations[32-35] have shown similar effects.

Direct experimental measurements of staging order have been somewhat more limited. Misenheimer and Zabel[36] found evidence for finite stage miscibility gaps in an *in situ* study of K-Gr; the size of the transition regions decreased with increasing stage. In another *in situ* study of staging in K-Gr, Nishitani *et al.*[37] claim to find no evidence of stage mixing up to stage 7. The apparent discrepancy of this result with our measurements will be discussed after the presentation of our data. The resistivity of the KC_x series has been measured by Phan *et al.*[38] The most striking feature of these measurements is the crossover from a positive temperature coefficient of resistivity for stages 4 and below to a negative temperature coefficient for stages 5 and 7. Small, hysteretic anomalies in the resistivity were interpreted as being due to in-plane structural transitions. In the stage-7 sample, the resistivity anomaly occurs at 235 K. Fuerst *et al.*[39,40] studied the c axis structure using x-ray and neutron diffraction to further investigate this anomaly. These measurements in-

dicated that the staging order was not perfect, but that their sample was a random mixture of 75% stage 7 and 25% stage 8 at room temperature, in qualitative agreement with the model of Kirczenow. Corresponding to the resistivity anomaly was an abrupt change to 90% stage 7. Recently, Kim *et al.*[41] have studied the structure of stages 1–3 K-Gr under pressure at room temperature. They observe both wide pressure regions in which the stage structure and disorder evolve continuously, and narrow pressure regions in which the average stage changes rapidly with pressure. The rapid stage changes are associated with in-plane structural transitions.

In this paper we describe a series of detailed x-ray diffraction measurements on stage 4 and higher potassium-intercalated graphite compounds, measuring both in-plane and out-of-plane structures. Our main findings are that the staging disorder increases with increasing stage, and that small discontinuous changes in the average stage are closely related to in-plane ordering transitions. Some of these results have been previously reported.[42,43]

Experimental details and methods of data analysis are given in Sec. II. In Sec. III we present our experimental results for samples of stage 6 and above, and in Sec. IV we present results for two stage-4 samples. Section V discusses the significance of our results.

II. EXPERIMENTAL TECHNIQUES AND ANALYSIS

A. Experimental techniques

Most of our samples consisted of highly oriented pyrolitic graphite (HOPG); two of the samples were natural, single-crystal Gr. All of the samples were intercalated with K via the standard two-zone technique, in which the Gr is heated and exposed to K vapor. The potassium was maintained at a temperature of 250 °C, while the Gr host was held at a temperature between 350 and 480 °C, depending on the desired stage. After approximately one day of exposure to K vapor, the samples were allowed to cool to room temperature over a period of several minutes. For fast characterization, samples were sealed inside pyrex ampoules which had walls about 1 mm thick. For more detailed measurements, the samples were mounted inside either thin-walled aluminum or beryllium sample cells. The interior of the cell was filled with argon to improve thermal contact with the sample. The samples were mounted either by gluing the sample directly to a phenolic post attached to the sample cell, or by wrapping the sample with aluminum foil which was then clamped to the cell; the second technique made it easier to re-intercalate the same Gr host but introduced aluminum peaks into the diffraction spectrum. The sample cells were then mounted on the cold finger of a Displex model 202W closed-cycle cryostat. The temperature was measured with a platinum resistance thermometer and controlled using a lock-in amplifier, Zilog Z8 single-chip microcomputer, a platinum resistance thermometer and a standard resistor in a bridge, and a wire resistance heater; this configuration controlled the sample temperature to within 0.1%.

Our diffraction measurements used the Mo $K\alpha$ radiation from a Rigaku Ru-200 rotating anode x-ray generator operating at 5 kW. Most measurements were made in a high intensity, low-resolution configuration, using the (00.4) reflection[44] from a 2-in. cylindrically bent HOPG monochromator before the sample and 0.10° Soller slits between the sample and a NaI scintillation detector. This low-resolution configuration, with a longitudinal resolution of about 0.01 Å^{-1} half width at half maximum (HWHM), was particularly important in measuring in-plane diffraction from K atoms in the high-stage samples, where the stoichiometry is approximately KC_{96} and hence the superlattice Bragg peaks are due to diffraction from only 1% of the atoms. For c-axis scans, selected measurements were made in a triple axis configuration, using germanium monochromator and analyzer crystals; the resolution in this case was approximately 0.0003 Å^{-1} HWHM. Since HOPG is cylindrically powder averaged, all available information can be obtained by measuring the diffraction in one reciprocal space plane, which we will call the H-L plane. The L direction is along the c axis, while scans done in the perpendicular H direction measure a circular powder average in the Gr basal plane. Typically scans were done with either $H=0$ (c-axis scans) or $L=0$ (in-plane scans). In a few cases measurements were made on a grid covering the entire H-L plane. For the single-crystal samples, some measurements were made covering a grid in the H-K plane (basal plane).

B. c-axis analysis

c-axis scans were analyzed by least-squares fits to various models for a partially disordered staging structure. One model for such disorder is a partially random sequence of different layers. Each layer, in our case, represents a package of a different stage with an appropriate form factor and thickness. Hendricks and Teller[45] (HT) derived an exact, analytic expression for diffraction from a one-dimensional, disordered lattice; this model was subsequently refined by Kakinoki and Komura.[46] The HT model describes the scattering for a restricted type of layer disorder, in which the system is described by the following two probabilities: first, the probability of finding a layer of type i at a point in the crystal, and second, the probability that the next layer will be a layer of type j given that the current one is of type i. These probabilities are denoted as f_i and P_{ij}, respectively. There are constraints on the probabilities:

$$\sum_{i=1}^{r} f_i = 1 ,$$

$$\sum_{j=1}^{r} P_{ij} = 1 ,$$

$$\sum_{i=1}^{r} f_i P_{ij} = f_j ,$$

where r is the number of layer types. These probabilities can be put into matrix form; for an infinite lattice the calculation of the diffracted intensity reduces to taking the trace of a product of matrices which include information about the form factor, phase shift (i.e., cell thickness) for each type of cell, and the probabilities. Details of this analysis are given in Ref. 43. For K-Gr, the phase shift

and form factor can be simply calculated using the C-C layer spacing c_0, the C-K-C layer spacing d_0, the number of C layers per package (i.e., the stage), the in-plane density of the K atoms, and the C and K atomic form factors.

The qualitative features of scattering from one dimensionally disordered systems include systematic shifts of peak positions from the indexed Bragg positions, anomalous broadening of some peaks but not others, and diffuse scattering between Bragg peaks. To take a specific example, consider a sample consisting of 75% stage-7 and 25% stage-8 packages, randomly mixed. Both the (00.8) peak of an ideal stage-7 crystal and the (00.9) peak of an ideal stage-8 crystal are close to 1.9 Å^{-1}, the pure Gr (00.2) position. Even though only stage-7—like peaks will appear, those peaks which are close to the "constructive interference condition," such as the (00.8) and the (00.16), will be relatively sharp and unshifted, whereas those peaks that are at substantially different positions from their stage-8 counterparts, such as the stage 7 (00.3), will be broadened and shifted in the direction of the nearest stage-8 peak. We give an explicit example of such broadening below. Fuerst and co-workers[39,40] compared the deviations of their peak positions from ideal Bragg indexing with the predictions of the HT model to calculate the fraction of each stage that was present. We have extended their analysis to perform least squares fts of *entire* diffraction profiles, resulting in greater sensitivity to the details of the disorder present.

Several variants of the HT model are used in analyzing our data. In some cases, we use a model employing a partially random mixture of two different layer types. We call this the "two-stage" model. In this case, two parameters are needed to completely describe the probability distribution, one determining the overall stoichiometry and the other determining the amount of disorder present. We choose the following parameterization of the probability matrix **P**:

$$\mathbf{P}=\begin{bmatrix} f_1(1-\alpha)+\alpha & f_2(1-\alpha) \\ f_1(1-\alpha) & f_2(1-\alpha)+\alpha \end{bmatrix},$$

$$\max\left[\frac{-f_i}{1-f_i}\right]\leq\alpha\leq 1\ ,$$

where $f_1=1-f_2$. The allowed values of f_1 and α and the dependence of stage structure on α and f_1 are shown schematically in Fig. 1. If $\alpha=1$, then the system has complete phase separation; a type one layer can only be followed by a type one layer and *vice versa*. As α is decreased, the layers become more mingled, and at $\alpha=0$ the two types of layer are randomly mixed. The probability of finding a type-1 layer after either type of layer is just the overall probability of finding a type-1 layer. On the other hand, when α becomes negative, the layer most likely to follow a type-1 layer is a type-2 layer; a heterostructure is formed of alternating layers. In a 50:50 mixture with $\alpha=-1$, the layers alternate perfectly. Figure 2 shows a sequence of calculated diffraction profiles for different α values in a mixture of stage-4 and stage-5 K-Gr. With decreasing α the calculated diffraction profiles evolve continuously from a sum of sharp stage-4 and stage-5 peaks to a highly disordered profile incorporating diffraction maxima from both structures.

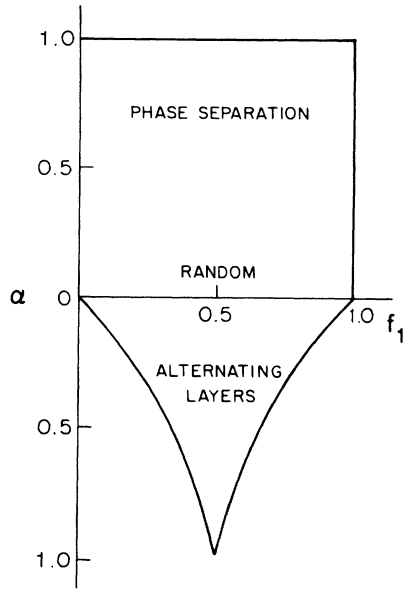

FIG. 1. The allowed values of f_1 and α, and the stage structure in the (f_1,α) plane for a two-phase Hendricks-Teller model.

As will be discussed in Sec. IV, we used a two-stage HT model with α large and positive (typically in the vicinity of 0.8) as a model for phase separation in stage-4 + stage-5 K-Gr. Strictly speaking, this model is an oversimplification. In a stage-4 + stage-5 two-stage model, although packages are correlated via the parameter α, the correlations are forced to be the same everywhere in the sample, i.e., the environment of a stage-4 package is assumed to be the same everywhere. For large α, the structure will consist of extended regions of pure stage 4 followed by ex-

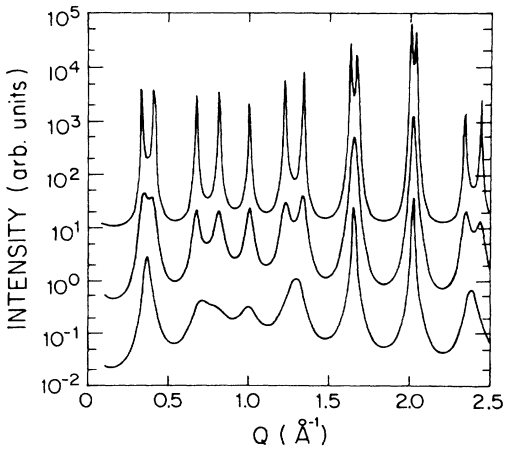

FIG. 2. Hendricks-Teller diffraction profiles for mixtures of 50% stage-4 and 50% stage-5, K-Gr. Upper: $\alpha=0.9$ (almost complete phase separation). Middle: $\alpha=0.5$. Lower: $\alpha=0.1$ (an almost completely random mixture). The scale has been offset by multiplying the middle and upper curves by 30 and 1000, respectively.

tended regions of pure stage 5. By contrast, in thermodynamic equilibrium such a system should consist of separated stage-4—rich and stage-5—rich regions. An improved model[41] to describe equilibrium phase separation would sum two independent two-stage HT models, with two sets of parameters f_i and P_{ij}. This model has the disadvantage that at least three new arbitrary fitting parameters are introduced, at the expense both of increased computational time and of reducing the uniqueness of the fit. We therefore have not pursued this approach.

We found that diffraction from higher stage samples could not be described by a random mixture of two different stage packages. Specifically, the experiments found more diffuse scattering between peaks than was predicted by the model. In an attempt to describe the additional disorder, two modifications of the above model were developed. This first modification is to add a third layer type to the model. Parametrizing the probabilities in this case is surprisingly tricky. Instead of one parameter describing the probability distribution, there are three. We chose a probability distribution in which two types of package are mixed with a variable amount of randomness, as above, and a third package type is mixed *completely* randomly with the other two. The probability parametrization is

$$\mathbf{P}=\frac{1}{1+\alpha f_3}\begin{bmatrix} f_1(1-\alpha)+\alpha & f_2(1-\alpha) & f_3 \\ f_1(1-\alpha) & f_2(1-\alpha)+\alpha & f_3 \\ f_1 & f_2 & f_3(1+\alpha) \end{bmatrix}.$$

We refer to this model as the three-stage model. (A similar algorithm appears to work well for pressure-induced disorder.[41])

An alternative modification of the basic HT model is to redefine the layers. Consider a model where the first layer is defined as a stage-5 K-Gr package, and the second layer is defined as a bare carbon layer. We will call this a "stage + carbon" model. If the probability of a stage-6 package is 0.5 and α is large and negative, then a stage-6 package will probably be followed by a bare C layer; the result is a stage-7 package. If more C layers follow then the stage will be higher. Using this definition of the layers, with the same number of variables as the two-stage model, yields a distribution of many different stage packages. The probability $G(n)$ of finding a package of stage n in a stage N +carbon model is

$$G(n)=\begin{cases} 0, & n<N \\ f_2(1-\alpha)+\alpha, & n=N \\ f_2 f_1(1-\alpha)^2[f_1(1-\alpha)+\alpha]^{n-N-1}, & n>N \end{cases}$$

where f_1 is the probability of a C layer and f_2 is the probability of a stage-N package. With this probability distribution the average stage and the standard deviation of the stage distribution are

$$\langle n\rangle = N+\frac{f_1}{f_2},$$

$$\sigma_n=(\langle n^2\rangle-\langle n\rangle^2)^{1/2}=\left[\frac{f_2(1+\alpha)}{f_1^2(1-\alpha)}\right]^{1/2}.$$

This probability distribution can peak at either stage N or stage $N+1$. It has a sharp cutoff at low stage and a long tail on the high stage side of the distribution. Fortunately, this is physically reasonable since the energy difference between stages gets smaller as the stage gets higher.[47] The stage probability function for a stage-6 + graphite HT model is shown in Fig. 3. Note that there is zero probability of finding a stage-5 package, but a nonzero probability of finding up to stage 12 and higher.

To give more flexibility in the distribution we also use a three package model with stage N, stage $N-1$, and C layers. For this model the $N-1$ package is a randomly distributed layer. In this case

$$\langle n\rangle = N+\frac{f_1-f_3}{f_2+f_3}$$

and

$$\langle n^2\rangle-\langle n\rangle^2=\frac{f_3(f_2+2f_1)-f_1^2}{(f_2+f_1)^2}-\frac{f_1(1+P_{11})-2f_3P_{31}}{(f_2+f_3)(1-P_{11})},$$

where f_1 is the probability of a C layer, f_2 is the probability of a stage-N package, f_3 is the probability of a stage-$(N-1)$ package, and P_{11} is the probability that a C layer will follow a C layer.

The probability of finding an intercalant layer of type-M stage-N package thicknesses away, $G_N(M)$, is approximately $G_{N-1}(M)G_1(M)$ if $G_1(m)$ is close to 1. Correlations between intercalant layers thus fall off like K^{-r} for some constant K; this type of probabilistic model implies either exponential correlations or perfect long-range order within each phase if $P_{ij}=\delta_{ij}$. The Fourier transform of an exponential correlation function yields an Lorentzian function, and thus well separated diffraction peaks in HT profiles have approximately Lorentzian shapes.

In fitting actual c-axis diffraction data, the bare HT line shape was convoluted with a Gaussian resolution function. (A Gaussian resolution function, $R(q-q_0)\propto\exp[(q-q_0)^2/\delta^2]$, is expected to provide a much better approximation to a mosaic-limited low-resolution instrumental configuration than to a Darwin width limited high-resolution configuration, and indeed the detailed line

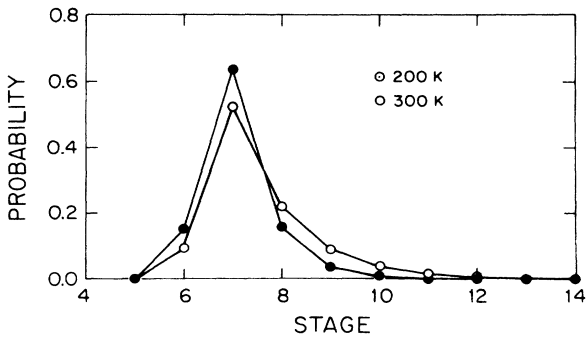

FIG. 3. Probability distribution derived from stage-6 + graphite HT fits to sample 1 (00.L) scans at 200 and 300 K.

shape fits worked much better for our low-resolution data than for our high-resolution data.) The convolution, which was somewhat time consuming, was done numerically using a variable step-size integration algorithm. The line shape was also multiplied by Lorentz and polarization factors. Several slowly varying factors, such as beam attenuation by the sample and illuminated volume effects, could not be calculated and were not included in our models. These slowly varying factors could empirically be modeled by a multiplicative factor of the form $q^{-\gamma}$, with γ allowed to vary. Figure 4 shows a c-axis diffraction scan from 0 to 8 Å^{-1}; the solid line is a two-stage model with all parameters allowed to vary, multiplied by $q^{-0.36}$. (Note that since our diffraction data show considerable dynamic range in intensity, we have used a logarithmic intensity axis in this and subsequent figures.) For most of our fits we did not include a $q^{-\gamma}$ factor, but simply restricted the range of the fits to the $0 \leq q \leq 3$ Å^{-1}.

We used the convolved HT line shapes to perform least-squares analysis of all our c-axis diffraction scans; the analysis was done on a LSI 11/23 microcomputer. In principle, the fitting parameters included the staging probabilities, a multiplicative factor for the scattered intensity, a term to correct for small errors in the centering of the diffractometer (2-θ offset), c_0 and d_0, the instrumental resolution, and a constant additive term representing background scattering. In practice, the instrumental resolution was held fixed at its measured value, and for sequences of fits to measurements on a particular sample the 2-θ offset, layer spacings, and background terms were held fixed at their average values. The goodness-of-fit parameter, χ^2, was quite sensitive to the value of the 2-θ offset, which always fit to less than $\pm 0.02°$, or less than 10% of a resolution half width. However, the other parameters were almost completely uncorrelated with this parameter. The layer spacings always came close to their nominal values of $c_0 = 3.35$ Å and $d_0 = 5.35$ Å.

Least-squares fits are done by numerically varying the independent parameters in a model to minimize the goodness-of-fit parameter χ^2, which is a sum of [(model − data) × weight]^2. In the present case, the weighting for each point is determined by Poisson statistics. Since there is considerable dynamical range on intensity and hence statistics in our c-axis scans, the fitting parameters tended to be determined by the detailed shape of the most intense peaks, rather than the overall shape of the entire diffraction profile. To mitigate this effect, we sometimes did fits with various parameters held fixed and chose as the best fit that which appeared by eye to conform best to the data over the *entire* range measured, rather than necessarily that which gave the best χ^2. Also, although we believe that the HT model contains most of the features needed to describe the data, there were still systematic differences between the model and the data. Therefore, if two otherwise identical scans were counted for different lengths of time fits to them would give different values of χ^2. Thus, although χ^2 was the figure of merit used by our programs in minimizing fitting parameters, it was not always useful to use it in comparing fits to different data sets.

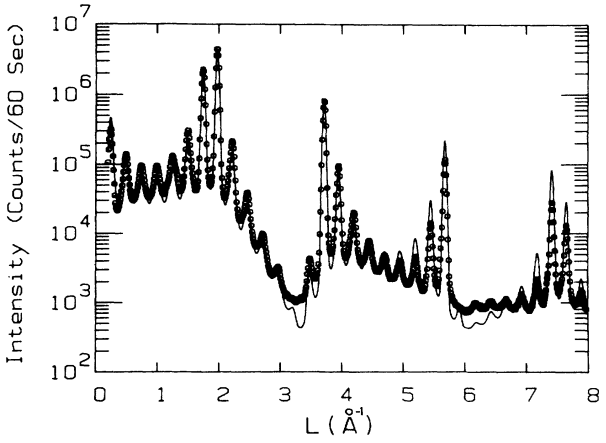

FIG. 4. c-axis scan on sample 1. Solid line is a HT stage-7 + carbon fit times $q^{-\gamma}$ with $\gamma = 0.36$.

C. In-plane analysis

In-plane peaks were fit to a variety of empirical models. Liquid structures have short-range order which may be expected to decay approximately exponentially; it was found that diffraction maxima in the disordered phase could be well described by Lorentzian line shapes. For commensurate 2D inplane structures with long-range order, the ideal scattering function is a Bragg rod, described as a δ function in the H direction and a slowly decaying function in the L direction. The ideal crystal δ-function peak is broadened by both finite-size effects and instrumental broadening; for our measurements, only the latter were important. Thus, commensurate inplane solid peaks were well described by resolution-limited Gaussian functions. An ideal incommensurate 2D inplane solid should display long-wavelength fluctuations resulting in a power-law cusp in the diffraction; this function, broadened by finite size in instrumental effects, can be effectively modeled by a Lorentzian lineshape.[48] Aside from the difference in peak position, a smeared power law line shape can be distinguished visually from a resolution-limited Gaussian by the higher degree of diffuse scattering in the tails of the peak. It was found necessary in all of our in-plane fits to add a background term due to air scattering, inelastic scattering from the sample, and other incoherent sources of diffraction. This background term was typically described as a slowly varying polynomial, the coefficients of which were determined by fits to a low-temperature scan and held fixed thereafter.

III. HIGH-STAGE SAMPLES

We studied over twenty K-Gr samples of stage 6 and above; we present data for five of these samples. (The nominal stage and host material for all of our samples is summarized in Table II.) Most samples we prepared from an HOPG host; one sample was prepared from natural, single-crystal Gr. Data from the first sample, 1, is described in more detail than the other samples because it

TABLE II. Nominal stage and host materials for intercalated samples.

Sample	Host	Nominal stage
1	HOPG	7
2	HOPG	7
3	HOPG	6
4	HOPG	8
5	Gr (single crystal)	11
6	HOPG	4
7	Gr (single crystal)	4

serves to illustrate most of the structural features found in samples with stages greater than 5. The results of the other samples are then presented, and differences from sample 1 are noted. For sample 1, we will first discuss the c-axis data, with emphasis on the different models used to describe the c-axis diffraction profiles. Then the change in c-axis structure is shown as a function of temperature, and finally the in-plane structure is presented and analyzed.

A. Sample 1

Sample 1, which was nominally stage 7, came from the same batch as the sample used by Phan *et al.*[38] in the first study of staging disorder in K-Gr. One large piece of HOPG was intercalated, then cut into several samples. We found that different samples from the original piece had slightly different average stage at room temperature, and thus different concentrations of intercalant. These samples had been stored at room temperature in sealed Pyrex ampoules for four years between preparation and measurement. It is possible that the observed variation in concentration is due to deintercalation in the slightly different environments of the different ampoules. Alternatively, the spread in concentrations might be due to inhomogeneities in the original intercalation process. We baked sample 1 inside its Pyrex ampoule, which contained no K, several times, making intermediate measurements of the c-axis structure. After each bake the concentration of K in the sample decreased slightly, but the diffraction profile was otherwise unchanged. We therefore infer that concentration inhomogeneities within *each sample* were not a problem.

Figure 5 shows c-axis scans from sample 1. (The additional scattering near 1.4 Å^{-1} is due to $2\lambda/3$ higher-order contamination of the beam.) As discussed in the analysis section, the $(00.n+1)$ peaks of stage n samples are close to the position of the pure Gr(00.2) peak, and thus these peaks are expected to be sharp even in a disordered mixture of many stages. In the present case, we find that the stage-7 (00.8) peak is resolution limited with a 0.025 Å^{-1} half width; this peak serves to determine our resolution function. The (00.4) peak has a halfwidth of 0.046 Å^{-1}. This width, if interpreted naively, would imply a correlation length of 19 Å; this distance is to be compared with the stage package thickness of 26 Å. Thus, this sample is highly disordered. The bottom half of Fig. 5 shows the results of a fit to the stage-7 + stage-8 two-stage HT

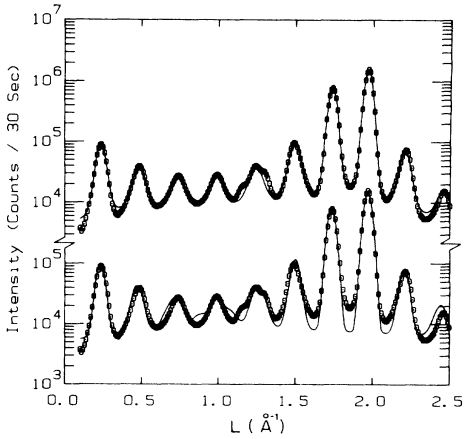

FIG. 5. Sample c-axis scan at 300 K fit with different HT models. Upper: stage + carbon HT fit. Lower: two-stage HT fit.

model. The ordering parameter α has been set to zero; fits in which α was allowed to vary gave slightly better χ^2 values but gave a considerably worse fit to the low-intensity peaks. It can be seen that the two-stage fit disagrees with the data in several regards. First, there several spurious peaks in the range 0.3–1.7 Å^{-1}. Second, although the peak intensities are in fair agreement with the data, the model underestimates the diffuse scattering between the peaks. By contrast, a fit to the stage-6 + carbon model, shown in the upper half of Fig. 5, is considerably better, although there are still a few systematic discrepancies. In general, we find that for samples of stage 6 and higher, the stage + carbon model describe the data better than the two-stage model, implying that these samples are highly disordered. Table III shows the results of baking on the sample 1. As discussed above, the average stage of the sample increased when it was baked. There was not much change in σ_n after the first bake, but it was significantly larger after the second bake.

Table IV shows parameters derived from fits to c axis scans between 0.1 and 2.5 Å^{-1} at four temperatures. At around 235 K there is a subtle but distinct change in the c-axis structure, with the average stage decreasing from 7.54 to 7.13 with decreasing temperature. Figure 3 shows the probability of different stage packages derived from the stage + graphite HT model at 200 and 300 K for this sample. The sum of all the probabilities must of course equal 1; as the temperature is lowered the average stage decreases and the probability distribution function also becomes more sharply peaked, implying a decrease in the disorder. The most dramatic change in the raw data is the intensity of the (00.1) peak, which shifts slightly in position and decreases by roughly 20% in intensity going through the transition. In characterizing the related in-plane transition, we monitored only the (00.1) peak at each temperature as an indication of change in the c axis structure. Fits to the long $(00.L)$ scans show that most of the other parameters do not change greatly with temperature, and show no anomalies at the transition. Figure 6

TABLE III. Effect of baking on sample 1. Parameters are "carbon-layer fraction" and "ordering" parameter for a stage-6 + carbon model, as described in text; $\langle n \rangle$ and σ_n are the average stage and width of the stage distribution function. Both the average stage and the stage disorder increase slightly upon annealing.

f_c	α	$\langle n \rangle$	σ_n	
0.562	−0.498	7.28	0.99	First measurement
0.566	−0.508	7.30	0.99	Baked at 200°C for 14 h
0.604	−0.498	7.53	1.14	Baked at 300°C for 21 h

shows the results of stage + carbon fits to the (00.1) peak as a function of temperature, with all parameters except the intensity, probability of a C layer, and ordering parameter α held fixed. Comparison to Table III shows that fits to the (00.1) peak alone yield results which are qualitatively similar, but numerically slightly different from fits to the entire spectrum up to 2.5 Å^{-1}. Note that the average stage changes quite abruptly by about 0.5 in a narrow temperature range between 235 and 245 K.

We now discuss the in-plane structure of sample 1. The temperature at which the c-axis structure changes abruptly corresponds to the in-plane solidification temperature. Above the transition there is only a broad fluid-like peak at 1.124 Å^{-1} (bottom of Fig. 7). The low-temperature in-plane structure is a two-dimensional, $\sqrt{7}\times\sqrt{7}$ commensurate solid (top of Fig. 7). The low-temperature in-plane superlattice K(H,K) peaks are resolution limited, implying that the in-plane spatial correlations extend over more than 250 Å. Analysis of the positions of the in-plane superlattice peaks and Gr(10.0) show that the superlattice is commensurate to better than 0.5%; the position of the lowest-order K(1,0) peak is 1.102(10) Å^{-1}. Indeed, all low-temperature superlattice peaks could be indexed to a commensurate $\sqrt{7}\times\sqrt{7}$ lattice, without additional peaks due to incommensurate modulations. Scans done through the K(1,0) peak in the L direction showed no evidence of a 0.25 Å^{-1} periodicity, as would be expected for a 3D superlattice. Rather, the slow variation of intensity of c-axis scans through the K(1,0) peak can be completely accounted for by the change in sample absorption and the evolution of the K atomic form factor with q.

Figure 8 shows the thermal evolution of the lowest-order K(1,0) peak. To analyze the in-plane data versus temperature, the 220-K K(1,0) peak was first fit to a Gaussian line shape plus a cubic polynomial, and this fixed background plus a Lorentzian line shape was used to fit the 240-K fluid peak. The rest of the scans were then fit to coexisting Lorentzian and Gaussian peaks, with the amplitudes of the peaks allowed to vary and the widths and positions of the two peaks fixed at their extremal positions. The results of these fits are shown in Fig. 9. The observation of coexisting sharp peaks (characteristic of the solid phase) and broad peaks (characteristic of the fluid phase), rather than a continuous evolution of the line shape, is expected for a first-order transition. We also observed a 5-K hysteresis in the temperature dependence of the peak positions, again consistent with a first-order transition.

TABLE IV. Results of stage + carbon fits to c-axis scans on sample 1 versus temperature: probability of carbon layer, "ordering" parameter, average stage, and stage distribution standard deviation.

T (K)	f_c	α	$\langle n \rangle$	σ_n
300	0.609	−0.493	7.56	1.16
273	0.610	−0.489	7.56	1.17
250	0.607	−0.540	7.54	1.08
200	0.531	−0.593	7.13	0.79

Note that the in-plane fluid expands on freezing. The shift in the K(1,0) peak position from 1.124 Å^{-1} to 1.102 Å^{-1} corresponds to a 2% increase in nearest-neighbor distance or a 4% decrease in in-plane density. The number of occupied galleries increases to compensate for this decrease in in-plane density. From Table IV, the fractional change in the number of occupied galleries is

$$\frac{\Delta N_i}{N_i}=\frac{0.41}{7.56}=0.05 .$$

Thus, within our experimental error the stoichiometry of the sample is conserved and remains constant upon repeated temperature cycling.

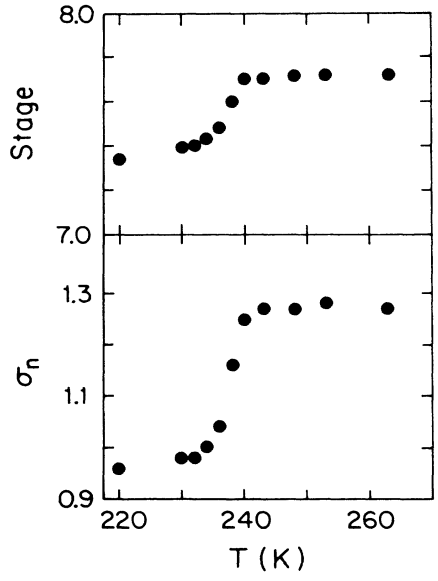

FIG. 6. Mean stage (upper) and standard deviation (lower) of stage distribution from fits to (00.1) peak of sample 1.

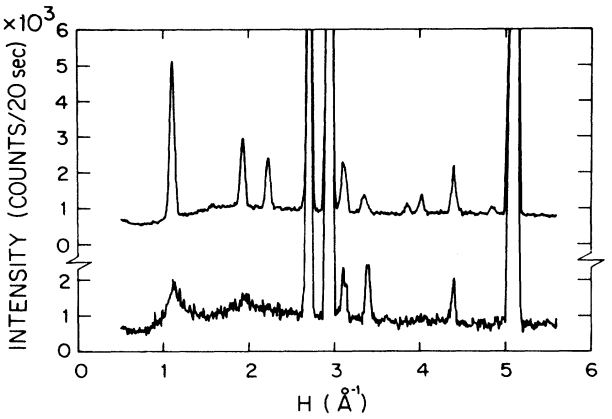

FIG. 7. In-plane diffraction scans from sample 1 at 200 K (upper) and 250 K (lower). (Lower temperature intensity has been rescaled because data were collected at lower power.) Sharp peaks found in both scans are due to Gr(10.0), Gr(11.0), and also Al diffraction peaks due to the sample container.

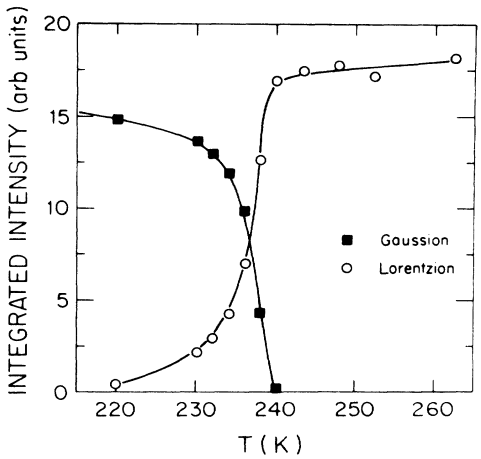

FIG. 9. Integrated intensities from Gaussian + Lorentzian coexistence fits to sample 1 K(1,0) peak. Solid points are Gaussian intensity; open points are Lorentzian intensity. (Intensity scale is arbitrary, but proportional to integrated intensity in the x-ray peak). Solid lines are guides to the eye.

B. Sample 2

We now discuss our measurements on sample 2. This was the original sample studied by Phan *et al.*[8] Low-resolution in-plane scans, and both low- and high-resolution c-axis scans, were measured for this sample.

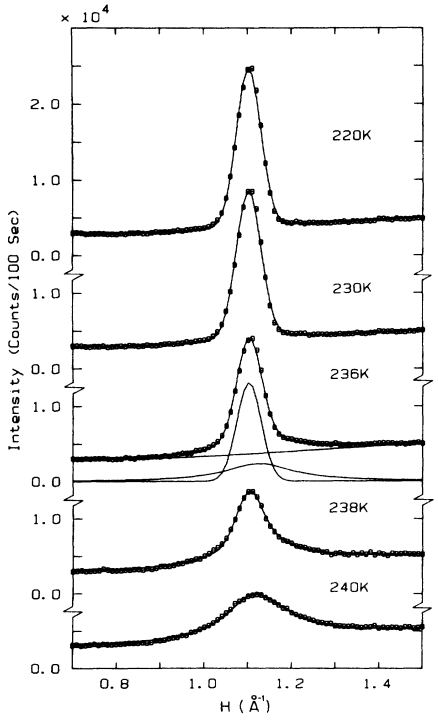

FIG. 8. Sample 1 K(1,0) diffraction peak in the vicinity of the melting transition. Solid lines are fit to a coexistence lineshape, as discussed in the text. Additional smooth, broadly peaked, and sharply peaked curves at 236 K are, respectively, the background, Lorentzian, and Gaussian components of the fitted line shape at this temperature.

Table V shows the results of fits to a Lorentzian line shape of high-resolution (00.L) scans. The peak widths vary by a factor of 30 from $\kappa=0.085$ Å^{-1} in the (00.4) peak to $\kappa=0.0033$ Å^{-1} in the (00.15) peak. This result is in qualitative agreement with the "constructive interference" mechanism for line shape broadening in disordered one-dimensional two-component crystals discussed above. Using the nominal values of $c_0=3.35$ Å and $d_0=5.35$ Å, the (00.15) peak of a stage-7 sample should lie at 3.7033 Å^{-1} and the (00.17) peak of a stage-8 sample should lie at 3.7088 Å^{-1}; the 0.0055-Å^{-1} splitting between these peaks is in good agreement with the resolution-limited 0.0033-Å^{-1} width of the (00.15) peak of the mixed-stage sample. By contrast, the (00.4) peak of an ideal stage-7 sample is at 0.9875 Å^{-1}, while the (00.4) and (00.5) peaks of a pure stage-8 sample are at 0.8727 and 1.0908 Å^{-1}, respectively, in agreement with the 0.085-Å^{-1} width of the mixed-stage (00.4) peak.

Extended Hendricks-Teller fits to sample 2 high-resolution scans were not very successful; this is most

TABLE V. Results of fits of sample 2 high-resolution 222 K (00.L) scans to a Lorentzian line shape, $I=A\kappa^2/[\kappa^2+(q-q_0)^2]$. The (00.6) peak could not be fitted due to higher-order contamination; the (00.10) through (00.14) peaks were too weak to be fit.

Index	Amplitude	q_0	κ
1	5.27	0.2350	0.016
2	1.28	0.4785	0.042
3	0.654	0.7285	0.076
4	0.510	0.9805	0.085
5	0.648	1.2461	0.064
7	30.4	1.7368	0.0076
8	79.4	1.9726	0.0043
9	0.628	2.2067	0.036
15	2.93	3.7232	0.0033

likely due to difficulty in correcting for geometrical sample absorption and illumination effects in the particular geometry that was employed.[49] Stage + carbon HT fits to the high-resolution scans gave values for the mean stage and stage distribution of $\langle n \rangle = 8.0$, $\sigma_n = 1.7$ at 239 K, and $\langle n \rangle = 7.4$, $\sigma_n = 1.3$ at 222 K; similar fits on low-resolution scans of sample 2 gave $\langle n \rangle = 7.7$, $\sigma_n = 1.3$ at 300 K and $\langle n \rangle = 7.3$, $\sigma_n = 0.9$ at 222 K. The differences between the two sets of fits are illustrative of the variations between HT fits using slightly different algorithms, sets of fixed parameters, or data sets: the exact values of mean stage, stage width, or other parameters may vary, but the shift to lower stage with decreasing temperature is not highly model dependent. Similarly, we found that fitting single peaks, rather than entire diffraction profiles, to HT line shapes yielded slightly different parameters, and in this case we feel that it is desirable, when possible, to analyze entire profiles. Indeed, it was the systematic discrepancy of the intensity *between* peaks, rather than peak positions or widths, that led us to develop the stage + carbon HT model.

The in-plane structure of sample 2 is the same as that of sample 1: the high-temperature two-dimensional fluid has a first-order transition to a $\sqrt{7} \times \sqrt{7}$ solid at around 235 K. We illustrate the transition by plotting the intensity of the (00.1) peak and the K(1,0) peak versus temperature (Fig. 10). Note the coincidence of the change in in-plane and out-of-plane structures, and the hysteresis in the transition.

Figure 11 is a contour plot of diffraction intensity in the entire H-L plane of sample 2. (The pattern is powder averaged about the L axis, so that all directions in the H-K plane are equivalent.) The vertical spine at $H=0$ is composed of the $(00.L)$ diffraction peaks, with stage-7 superlattice periodicity. The tails of the c-axis mosaic are seen clearly around the strong (00.8) peak (2×10^5 counts/sec max), extending almost 45° from the $H=0$ direction. The three smooth ridges at $H=1.1$ Å^{-1} (290 counts/sec), $H=1.9$ Å^{-1} (120 counts/sec), and $H=2.2$ Å^{-1} (90 counts/sec) are, respectively, the (1,0), (1,1), and (2,0) Bragg rods due to 2D in-plane ordering of the K atoms. The vertical spine at $H=2.95$ Å^{-1} is the Gr $(10.L)$ diffraction profile; the modulation of the intensity along the $(10.L)$ direction is due to the $ABAB$ stacking of the C layers and also the stage-7 superlattice. [Recent work by Nishitani *et al.*[50] has shown that the stacking order of graphite and K layers is $|(AB)_{n/2}|(BC)_{n/2}|(CA)_{n/2}|$ for even-stage compounds and $|A(BA)_{(n-1)/2}|A(CA)_{(n-1)/2}|$ for odd-stage compounds, i.e., the stacking sequence alternates between odd- and even-stage compounds.] These periodicities are washed out to some extent by the c-axis mosaic and are also affected by stacking fault disorder. The irregular rings with radii of 2.65 and 3.1 Å^{-1} are due to scattering from aluminum in the sample cell.

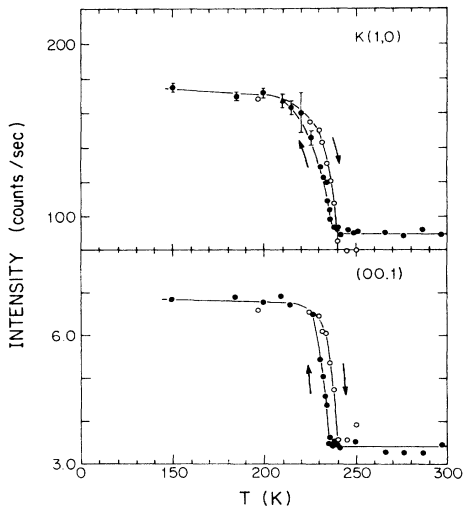

FIG. 10. Sample 2 fitted peak intensities versus temperature. Upper: intensity of in-plane K(1,0) peak. Lower: intensity of c-axis (00.1) peak. Arrows indicate the path taken.

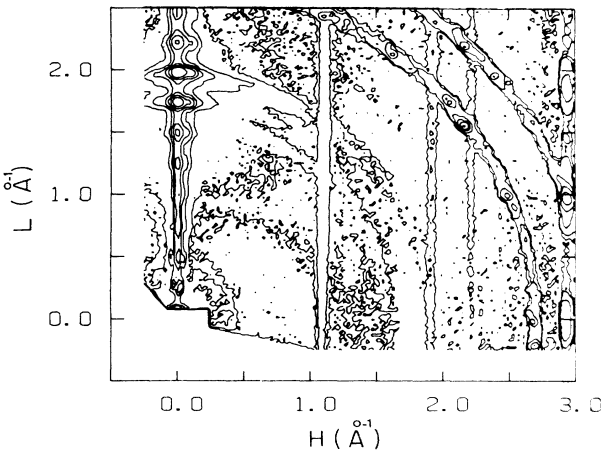

FIG. 11. Contour plot of diffracted x-ray intensity from sample 2 at 200 K. Contours are given at 100 000, 31 620, 10 000, 3162, 1000, 316, 100, and 66 counts/sec.

C. Sample 3

Sample 3 consisted of nominal stage-6 K-HOPG. The upper half of Fig. 12 shows two-stage and stage + carbon fits to c-axis scans of sample 3. The stage + carbon fit (b) clearly reproduces the observed peak-to-valley ratio better than the two-stage fit (a). A three-stage fit incorporating a small *random* mixture of stage-5 packages did not improve the fits. The sharp peak at ~ 1.4 Å^{-1} is due to higher-order contamination of the beam. The two-stage HT fits yield $\langle n \rangle = 6.35$, $\sigma_n = 0.48$ at 300 K and $\langle n \rangle = 6.17$, $\sigma_n = 0.38$ at 150 K, while the stage + carbon model yields $\langle n \rangle = 6.35$, $\sigma_n = 1.10$ at 300 K and $\langle n \rangle = 6.08$, $\sigma_n = 1.00$ at 150 K. A better model to the data would probably involve mixing a small amount of almost pure stage 5 with larger amounts of more disordered stage 6 and stage 7, with $\sigma \approx 0.9$; in any case we can conclude that the stage distribution is less broad at nominal stage 6 than at stage 7, and that the shift to lower average stage with lower temperature is still observed. The average stage is relatively constant between 300 and 243 K,

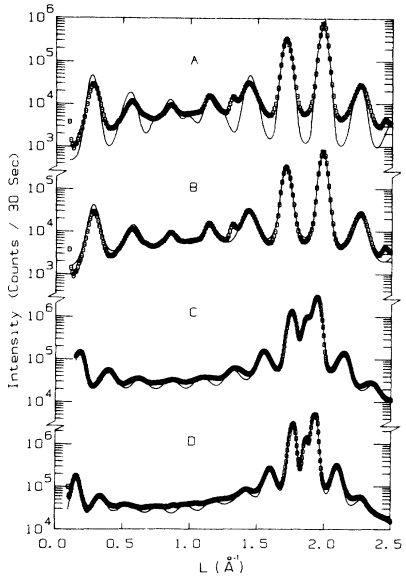

FIG. 12. c-axis scans for various samples. Solid lines are fits to HT models. (A) Sample 3, $T=150$ K; solid line is stage 6 + stage 7 model. (B) Sample 3, $T=150$ K; solid line is stage 6 + carbon model. (C) Sample 4, room temperature; solid line is a stage 7 + carbon model, with an additional Gaussian peak at 1.881 Å^{-1}. (D) Sample 5, room temperature; solid line is a stage 10 + stage 9 + carbon model, with an additional Gaussian peak at 1.876 Å^{-1}.

then drops sharply over a 20-K range as in-plane freezing occurs.

The in-plane structure of sample 3 is virtually identical to that of higher-stage samples. At high temperatures, the in-plane diffraction is well described by a Lorentzian, while at lower temperatures a series of $\sqrt{7}\times\sqrt{7}$ Gaussian peaks appear. The evolution in in-plane line shape is again better described by coexisting sharp Gaussian and broad Lorentzian peaks than by a single peak with evolving width. The transition is quite broad, with the coexistence between peaks beginning at 240 K and continuing to 210 K, and shows a 5-K hysteresis.

D. Sample 4

Sample 4 was drawn from the same batch of K-HOPG as samples 1, 2, and 3, and was nominally stage 8. Curve C in Fig. 12 shows a room-temperature c-axis scan. The solid line is an HT stage-7 + carbon fit with an additional Gaussian peak inserted at 1.881 Å^{-1}, the position of the pure Gr(00.2). Although this line shape has peaks in the right places, the peak-to-valley ratio is clearly too large between 0.3 and 1.4 Å^{-1}, indicating that the HT model is not sufficiently disordered. The pure Gr peak intensity is 34000 counts/sec and the superlattice (00.9) peak intensity is 98000 counts/sec. This sample appears to be composed of approximately 25% pure Gr plus highly disordered stage 8. We were unable to prepare any HOPG sample with nominal stage higher than 8. If the same sample was kept inside its pyrex container and repeatedly baked, the fraction of pure Gr increased relative to the stage-8 component. (The baking was done by heating the sample to ~300 °C overnight and then quenching to room temperature.)

E. Sample 5

Curve D in Fig. 12 shows a c-axis diffraction scan from sample 5, a natural, single crsytal of Gr intercalated to nominal stage 11. The solid line is an HT model incorporating stage-10 packages, stage-9 packages, and pure C layers, as well as an additional Gaussian peak at 1.876 Å^{-1}. The fit gives $\langle n\rangle=10.9$, $\sigma_n=2.17$, and it is again clear that this fit does not incorporate nearly enough disorder to account for the flatness of the diffraction profile. In this case the estimated percentage of pure Gr in the sample is 21%, based on the peak heights. In plane, the position of the K(1,0) peak is 1.11(1) Å^{-1} rotated 19(±4) degrees from the 2.92(±1)-Å^{-1} Gr(10.0) peak. Thus, the in-plane structure is a $\sqrt{7}\times\sqrt{7}R$ 19.1° superlattice. The in-plane superlattice melts at 240 K. Scans done in the c-axis direction through the K(1,0) peak showed no evidence of three-dimensional ordering down to 40 K.

The observation of coexistence between pure Gr and staged structures requires some discussion. We think it is unlikely that this coexistence is an equilibrium condition, because the interaction between the intercalant galleries is repulsive; there is no mechanism to keep intercalant atoms from invading a pure Gr region. It is more likely that the samples are being observed during the very slow process of deintercalation. Presumably the area near the surface of the samples consists of pure Gr, while deeper areas have not yet deintercalated. The observation that single-crystal hosts, which have longer in-plane coherence lengths than HOPG, can support higher staged structures is in general agreement with the model of Kirczenow.[30]

To summarize our results for high-stage samples: The c-axis structure of all samples with stage 6 and above was better described by a stage + carbon model than the more ordered two-stage HT model. The stage disorder increases with increasing stage. An in-plane fluid structure freezes to a commensurate $\sqrt{7}\times\sqrt{7}$ solid at 235 K; the coexistence of sharp and broad peaks and the hysteresis observed in the evolution of the diffraction are consistent with a first-order transition. The expansion of the in-plane lattice upon freezing forces a shift to lower average state to conserve sample stoichiometry. Perhaps coincidentally, this shift to lower average stage always appears to be accompanied by a shift to smaller stage distribution, i.e., a slightly purer phase.

IV. LOW-STAGE SAMPLES

We studied two stage-4 + stage-5 K-Gr samples, one using HOPG as a host material and one using single-crystal graphite. In both cases we found that a dramatic shift to lower stage at around 150 K was correlated with an in-plane freezing transition into an incommensurate superlattice.

A. Sample 6

We discuss first our measurements on sample 6, which consisted of stage-4 + stage-5 K-HOPG. The contour plot in Fig. 13 shows 3D $(00.L)$ and $(10.L)$ peaks, and 2D Bragg rods due to in-plane ordering of the K atoms. The in-plane structure is not commensurate; the strong peaks at $H=1.13$ and 2.26 Å^{-1}, and the weak peak at 1.96 Å^{-1}, index as incommensurate superlattice (1,0), (2,0), and (1,1) peaks. The low-temperature K(1,0) peak, as measured in both high- and low-resolution configurations, is better described by a resolution-limited Lorentzian with $Q=1.13$ Å^{-1} than by a Gaussian, consistent with the power-law line shape expected in a 2D incommensurate lattice.[48] The strong peak at $H=1.85$ Å^{-1} is most likely a (1,0) modulation peak around the Gr(10.0). Between 130 and 170 K the K(1,0) peak gradually broadens and decreases in intensity. At high temperatures, scans in the $(HK0)$ plane reveal a liquidlike peak corresponding to a lower density than that observed by Mori *et al.*;[11] a Lorentzian fit to this peak yields $Q=1.144$ Å^{-1} and $\kappa=0.13$ Å^{-1}, implying that the in-plane lattice expands upon freezing as seen in the high-stage samples.

Figure 14 shows the evolution of c-axis structure in sample 6 as a function of temperature. HT analysis of these scans shows that the c-axis structure is best described as a partially ordered mixture of stage-4 and stage-5 packages, with $\alpha=0.75$, corresponding to a simple model for phase separation of stage-4 and stage-5 regions. The addition of a third package did not significantly improve the fits; fits with the stage + carbon model were significantly worse. With decreasing temperature, fits to low-resolution scans show that the sample evolves from 54% stage 4 to 60% stage 4 between 300 and 200 K, and then changes rapidly to 75% stage 4 as the temperature is lowered to 150 K (Table VI). The evolution from stage 4.54 to 4.27 implies a 5% decrease in the number of K layers to unit length. HT fits to high-resolution $(00.L)$ scans from this sample showed the same trends as fits to the low-resolution data, although the agreement was not as good; this discrepancy is most likely due to difficulty in modeling the resolution function for a high-resolution configuration, as described above. The evolution in the fraction of stage-4 packages is somewhat larger in this case (Table VI).

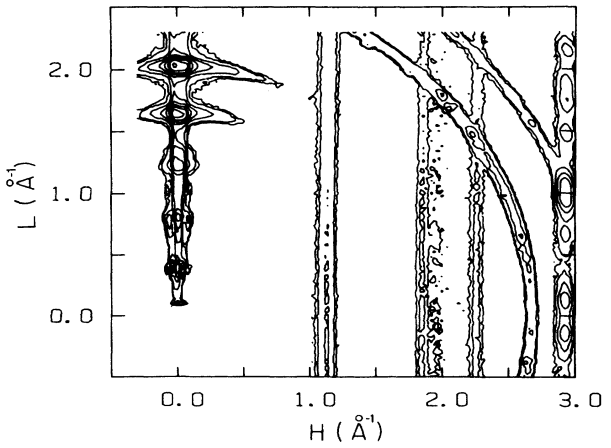

FIG. 13. Contour plot of x-ray intensity in $(H0L)$ plane of stage-4 + stage-5 K-HOPG (sample 6) 105 K. Contours are at 316 200, 100 000, 31 620, 10 000, 3162, 1000, 316, 100, and 66 counts/2 sec. Semicircular contours about $q=2.7$ and 3.1 Å^{-1} are due to scattering from the Al sample cell.

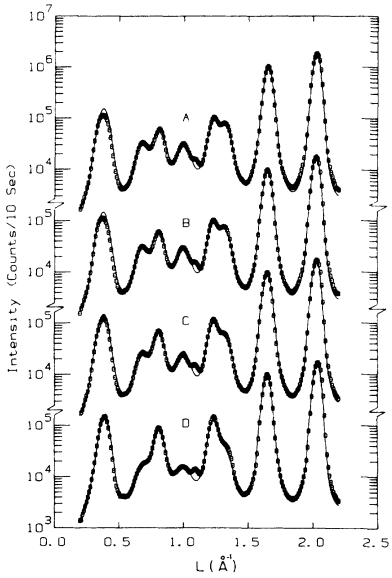

FIG. 14. Low-resolution c-axis scans, sample 6 (stage-4 + stage-5 K-HOPG). Temperatures are (A) 250 K, (B) 200 K, (C) 180 K, and (D) 105 K. Solid lines are stage-4 + stage 5 two-package HT fits, as discussed in the text.

TABLE VI. Results of fits to stage 4 + stage 5 K-HOPG $(00.L)$ scans to a two package HT model: probability of a stage-4 package, "ordering parameter," average state, and sequence (low or high resolution).

Temperature (K)	f_4	α	$\langle n \rangle$
	Low resolution		
300	0.542	0.269	4.46
250	0.585	0.369	4.42
225	0.587	0.367	4.41
200	0.597	0.366	4.40
180	0.631	0.364	4.37
150	0.746	0.301	4.26
105	0.746	0.301	4.26
	High resolution		
300	0.453	0.419	4.54
290	0.443	0.426	4.56
200	0.535	0.376	4.47
190	0.547	0.369	4.45
179	0.616	0.343	4.38
170	0.647	0.341	4.35
107	0.750	0.323	4.25
40	0.735	0.285	4.27

B. Sample 7

Diffraction scans in sample 7, a single Gr crystal intercalated to stage 4 + stage 5, confirm our identification of an incommensurate in-plane superlattice structure. In-plane diffraction spots can be indexed as primary Gr(10.0) and Gr(11.0) peaks at 2.94 and 5.16 Å^{-1}, primary superlattice peaks from a triangular lattice with $q_0 = 1.17$ Å^{-1} rotated $19 \pm 2°$ from the Gr(10.0) direction, and (1,0) modulation peaks about the Gr(10.0) and Gr(11.0) primaries. (Our resolution was not sufficient to allow us to unambiguously distinguish primary and modulation peaks in most cases; further measurements are anticipated.) Note that the primary incommensurate lattice is quite close to the $\sqrt{7}\times\sqrt{7}R$ 19.1° commensurate lattice, with reciprocal-lattice constant 1.11 Å^{-1}.

As the temperature is increased, the in-plane superlattice peaks and their angular widths increase to eventually form an orientationally ordered ("hexatic") in-plane fluid. Figure 15 shows a set of longitudinal scans through the K(1,0) peak as a function of temperature. Fits to the low-temperature line shapes yielded ambiguous results. The solid lines in Fig. 15 are the results of fits to a Lorentzian line shape with a fixed polynomial background; the background function was fixed by fits at low temperature. Such fits yield a quantitative measure of the temperature evolution of peak position and width, although the Lorentzian line shape does not describe the data perfectly. Likewise, a Gaussian line shape did not perfectly reproduce the diffraction profiles; it seems likely that the best function would be a smeared power-law line shape. Alternatively, a line shape consisting of a linear sum of characteristic low-temperature and high-temperature line shapes gives a comparable fit to the data. We therefore cannot distinguish from these measurements, which were done with relatively low instrumental resolution, between a smeared first-order transition and a truly continuous freezing transition. In fact, the observed temperature evolution of correlation length (Fig. 16) is very similar to that observed in low-resolution scans of the melting transition of 2D xenon adsorbed on the surface of graphite; in that case higher-resolution scans[48,51–53] have shown that the incommensurate superlattice melts into a hexatic fluid via a second-order transition. This similarity in the spectra would suggest that the present transition is also continuous, although the hysteresis of the electrical resistivity over a broad region of temperature[38] would argue for a possibly smeared first-order transition. Future high-resolution synchrotron studies may help to resolve this issue. Note that the change in character of the freezing transition from stages 4–7 can be explained by the change of symmetry of the low-temperature phase. The high-stage freezing transition to a $\sqrt{7}\times\sqrt{7}$ commensurate solid can be described by a seven-state Potts model; such a transition must be first order.[54] By contrast, the stage 4–5 freezing transition to a modulated incommensurate structure could be first order, but it could also occur via a second-order transition of the Kosterlitz-Thouless[55] type. No out-of-plane correlations were seen in either of our stage 4 + stage 5 samples down to 45 K. We can thus set an upper limit of $n = 4$ for the appearance of 3D effects at low temperature in K-Gr.

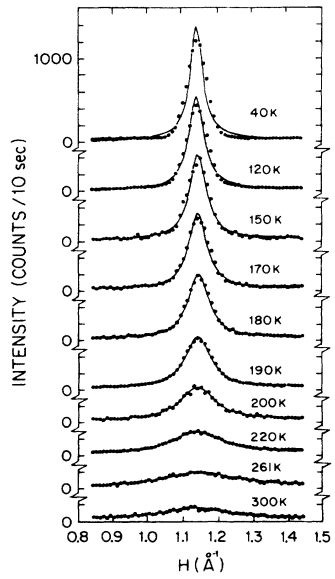

FIG. 15. Sample 7 (single-crystal K-Gr) K(1,0) diffraction peaks. Solid lines are results of Lorentzian fits as described in the text.

V. DISCUSSION

Analysis of our (00.L) scans shows that stage 4 + stage 5 samples are best described by a partially random mixture of two package types, while samples of stage 6 and greater are best described by a mixture of *many* package types. The trend to increased package miscibility at higher stage areas agrees qualitatively with the staging model of Kirczenow.[30] In all samples with stage $n \geq 4$, a sudden decrease in average stage occurs at the same temperature (and shows the same hysteresis, if any) as the in-plane transition. Indeed, the $6\% \pm 2\%$ decrease in in-plane density upon freezing agrees within experimental error with the 2–4 % increase in out-of-plane density, suggesting that the system increases the number of filled galleries to compensate for the decreased number of K atoms

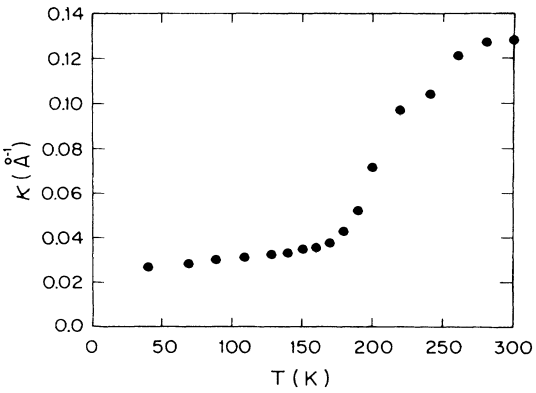

FIG. 16. Values of κ (inverse correlation length) from Lorentzian fits to sample 7 K(1,0) peaks.

in each gallery. The complementary effect has been seen in K-Gr at high pressure[23,57] and Li-Gr at low temperature[57] in which the number of filled galleries is decreased to maintain sample stoichiometry as the intercalants form a denser in-plane structure.

The c-axis structure of all samples with stage 6 and above was better described by a stage + carbon model than by the more ordered two-stage HT model. This implies that, at high mean stage, pure staging structures do not exist—the equilibrium structure is a disordered mixture of several package types.[1] The stage disorder increases with increasing stage. An in-plane fluid structure freezes to a commensurate $\sqrt{7}\times\sqrt{7}$ solid at 235 K; the coexistence of sharp and broad peaks and the hysteresis of the diffraction are consistent with a first-order transition. We found no high-stage K-C compound which produced resolution limited $(00.L)$ peaks, even though all high-stage compounds had a $\sqrt{7}\times\sqrt{7}$ in-plane structure. This implies that high-stage K-C will not form an ordered staging structure even if the stoichiometry should happen to be KC_{14n} for some integer n. The expansion of the in-plane lattice upon freezing forces a shift to lower average stage to conserve sample stoichiometry. This is the opposite of the trend to higher stage at lower temperature predicted by Safran's model,[20] which neglected in-plane interactions. This shift to lower average stage appears to be always accompanied by a shift to a narrower stage distribution, i.e., a slightly purer phase. This could be a true thermal reduction in the entropy of stage disorder, or it could be related to the fact that coincidentally all our samples had stoichiometry slightly greater than some mean integer stage rather than slightly less.

The observation of coexistence between pure Gr and staged structures requires some discussion. It is possible that we are observing a "maximum" stage of 11 for single-crystal hosts and 8 for more highly-disordered hosts. The observation that single-crystal hosts, which have longer in-plane coherence lengths than HOPG, can support higher staged structures is in general agreement with the model of Kirczenow.[30] The energetic basis of a maximum stage is unclear; there is no mechanism which would keep intercalant atoms from invading a pure Gr region. However, there are several effects which could account for the observed coexistence. We may be observing spatial inhomogeneity due to the intercalation process. Presumably, the area near the surface of the samples consists of pure Gr, while deeper areas have not yet deintercalated. (Alternatively, the surface may "pin" staged structures while the interior may reflect the true dilute equilibrium state.) It is also possible that inhomogeneous strains or defects could prevent intercalation of some regions in the high-stage regime, where intercalation is barely favored energetically in any case. This would account for the higher stages produced by the more pure graphite hosts.

Moss *et al.*[58] have suggested that transverse phonons from misoriented crystallites may contribute to the diffuse scattering between 0 and 2 Å^{-1} and distort the parameters obtained from HT fits. Indeed, there are a number of such effects that we have not included, including q-dependence of the background scattering, the detailed shape of the resolution function, geometric illumination and attenuation factors, and multiple scattering, all of which become important when diffraction measurements over several orders of magnitude in intensity are analyzed. As discussed above, the parameters obtained from the fits tend to depend somewhat on the model employed, and the range of data included. On the other hand, our primary results, that the staging disorder increases with increasing stage and that there is a shift to lower stage at the melting transition, are relatively insensitive to the details of our fits.

Since our measurements were made on samples that had been quenched rather than high-temperature *in situ* samples, detailed comparison with *in situ* measurements is difficult. Nevertheless, our observation that a sample containing coexisting stage-4 and stage-5 phases must be described using a model for disordered phase separation appears to be consistent with the recent *in situ* measurements of Misenhiemer and Zabel,[36] which showed increased stage disorder with increasing stage and a miscibility gap at the stage-4 to stage-5 transition. Nishitani *et al.*[37] have performed *in situ* energy-dispersive diffraction measurements of K-HOPG up to stage 7. They observe that all the $(00.L)$ diffraction peaks case be assigned to one or two diffraction peaks, and thence argue that there is no microscopic mixture of two stages up to stage 7, in contradiction to our observation of substantial stage disorder above stage 6. However, as long as the mean stage is well defined the primary effect of stage disorder is to broaden selected peaks and increase the amount of diffuse scattering. The Nishitani *et al.* experiments were done with fairly low momentum resolution and would not have been sensitive to such disorder. Their measurements *do* provide evidence for finite miscibility gaps even up to quite high stage.

As Table I shows, there is a general trend in K-Gr compounds for the in-plane density to decrease and, except for stage 1, the freezing transition temperature to increase with increasing stage. Thus, the change from stoichiometry KC_8 at stage $n=1$ to approximate stoichiometry KC_{12n} for higher stages is simply part of a general trend to lower in-plane density with increasing stage, with the biggest jump occurring as expected between $n=1$ and $n=2$. KC_8 is the only stoichiometric member of the K-GIC family; its 3D melting transition does not involve coupling between in-plane and out-of-plane densities.[37] At the dilute extreme, average stage 6 or higher, we found ground-state structures in which non-stoichiometry is accommodated by stage disorder while the in-plane density is clamped by the commensurate $\sqrt{7}\times\sqrt{7}$ superlattice. Intermediate cases such as KC_{24} probably exist in a variety of ground states, depending on the specific K/C ratio. This view is supported by the differing results obtained on supposedly the same compound by different groups.[59,60] It is unclear at this point whether these ground states are stabilized by in-plane or interlayer interactions. The *increase* of the freezing transition temperature with increasing stage is contrary to a simple mean-field picture in which as the K layers evolve from a 3D structure to a quasi-2D structure the freezing transition should decrease in temperature. It appears like-

ly that the energy scale of the freezing transition is set primarily by in-plane interactions, with commensurate structures melting at higher temperature than incommensurate ones.

ACKNOWLEDGMENTS

We would like to thank David P. DiVencenzo, Carl D. Fuerst, Hyun Joong Kim, George Kirczenow, Sasuka Miyazima, Simon C. Moss, and Samuel Safran for many useful discussions. We thank Zhi-Jiang Hang for his help in sample preparation and characterization. The graphite samples were generously provided by Arthur Moore (Union Carbide). This work was supported by the University of Pennsylvania and by the National Science Foundation Materials Research Laboratory Program under Contract No. DMR-8519059.

---

*Present address: Energy Science Laboratories, P.O. Box 85608, San Diego, CA 92138-5608.

[1]S. A. Solin, Adv. Chem. Phys. **49**, 455 (1981).

[2]R. Clarke, in *Phase Transformations in Solids,* edited by T. Tsakalakos (Elsevier, New York, 1984).

[3]M. S. Dresselhaus and G. Dresselhaus, Adv. Phys. **30**, 139 (1981).

[4]H. Zabel and P. C. Chow, Comments Solid State Phys. **12**, 225 (1986).

[5]S. A. Safran, in *Modulated Structure, Solid State Physics,* edited by F. Seitz, D. Turnbull, and H. Ehrenreich (Academic, New York, 1986).

[6]D. P. DiVincenzo and E. J. Mele, Phys. Rev. B **27**, 2458 (1983); **29**, 1685 (1984).

[7]R. Nishitani, Y. Uno, H. Suematsu, Y. Fujii, and T. Matsushita, Phys. Rev. Lett. **52**, 1504 (1984).

[8]D. E. Nixon and G. S. Parry, J. Phys. D **1**, 291 (1968).

[9]J. M. Bloch, H. Katz, V. B. Cajipe, and J. E. Fischer, Phys. Rev. B **31**, 6785 (1985),

[10]J. B. Hastings, W. D. Ellenson, and J. E. Fischer, Phys. Rev. Lett. **42**, 1552 (1979).

[11]M. Mori, S. C. Moss, Y. M. Jan, and H. Zabel, Phys. Rev. B **25**, 1287 (1982); M. Mori, S. C. Moss, and Y. M. Jan, Phys. Rev. B **27**, 6384 (1983).

[12]F. Rousseaux, R. Moret, D. Guerard, P. Lagrange, and M. Lelaurain, J. Phys. Lett. **45**, L1111 (1984).

[13]R. Clarke, N. Caswell, S. A. Solin, and P. M. Horn, Phys. Rev. Lett. **43**, 2018 (1979).

[14]M. Suzuki, H. Ikeda, H. Suematsu, Y. Endoh, H. Shiba, and M. T. Hutchings, J. Phys. Soc. Jpn. **49**, 671 (1980); M. Suzuki and H. Suematsu, J. Phys. Soc. Jpn. **52**, 2761 (1983).

[15]H. Zabel, Y. M. Jan, and S. C. Moss, Physica **99B**, 453 (1980).

[16]S. B. DiCenzo, Phys. Rev. B **26**, 5878 (1983).

[17]M. B. Gordon, J. Villain, and R. Clarke, Phys. Rev. B **25**, 7871 (1982).

[18]M. Suzuki and H. Suematsu, J. Phys. Soc. Jpn. **52**, 2761 (1983).

[19]Y. Yamada and I. Naiki, J. Phys. Soc. Jpn. **51**, 2174 (1982); I. Naiki and Y. Yamada, *ibid.* **51**, 257 (1982).

[20]S. Safran, Phys. Rev. Lett. **44**, 937 (1980).

[21]L. Pietronero, S. Strassler, H. R. Zeller, and M. J. Rice, Phys. Rev. Lett. **41**, 763 (1978); L. Pietronero, S. Strassler, and H. P. Zeller, Solid State Commun. **30**, 399 (1970).

[22]P. Bak and R. Bruinsma, Phys. Rev. Lett. **49**, 249 (1982).

[23]C. D. Fuerst, J. E. Fischer, J. D. Axe, J. B. Hastings, and D. B. McWhan, Phys. Rev. Lett. **50**, 357 (1983).

[24]K. C. Woo, H. Mertwoy, J. E. Fischer, W. A. Kamitakahra, and D. S. Robinston, Phys. Rev. B **27**, 7831 (1983).

[25]S. E. Millman and G. Kirczenow, Phys. Rev. B **28**, 3482 (1983).

[26]G. Forgacs and G. Uiman, Phys. Rev. Lett. **52**, 633 (1984).

[27]S. A. Safran and D. R. Hamann, Phys. Rev. B **22**, 606 (1980).

[28]P. Hawrylak and K. R. Subbaswamy, Phys. Rev. B **28**, 4851 (1983).

[29]J. R. Dahn, D. C. Dahn, and R. R. Haering, Solid State Commun. **42**, 179 (1982).

[30]G. Kirczenow, Phys. Rev. Lett. **52**, 437 (1984); Phys. Rev. B **31**, 5376 (1985).

[31]D. P. DiVincenzo and T. C. Koch, Phys. Rev. B **30**, 7092 (1984); D. P. DiVincenzo, Ph.D. thesis, University of Pennsylvania, 1983.

[32]G. Kirczenow, Synth. Met. **12**, 143 (1985).

[33]P. Hawrylak and K. R. Subbaswamy, Phys. Rev. Lett. **53**, 2098 (1984).

[34]S. Miyazima and T. Tanaka (unpublished); S. Miyazima, Synth. Met. **12**, 155 (1985).

[35]H. Miyazaki, Y. Kuramoto, and C. Horie, J. Phys. Soc. Jpn. **53**, 1380 (1984); H. Miyazaki and C. Horie, Synth. Met. **12**, 149 (1985).

[36]M. E. Misenheimer and H. Zabel, Phys. Rev. Lett. **54**, 2521 (1985).

[37]R. Nishitani, Y. Uno, and H. Suematsu, Phys. Rev. B **27**, 6572 (1984).

[38]K. Phan, C. D. Fuerst, and J. E. Fischer, Solid State Commun. **44**, 1351 (1982).

[39]J. E. Fischer, C. D. Fuerst, and K. C. Woo, Synth. Met. **7**, 1 (1983).

[40]C. D. Fuerst, T. C. Koch, J. E. Fischer, J. D. Axe, J. B. Hastings, and D. McWhan, in *Intercalated Graphite,* edited by M. S. Dresselhaus, G. Dresselhaus, J. E. Fischer, and M. S. Moran (North-Holland, New York, 1983), p. 39.

[41]H. J. Kim, J. E. Fischer, D. B. McWhan, and J. D. Axe, Phys. Rev. B **33**, 1329 (1986); H., J. Kim, Ph.D. thesis, University of Pennsylvania, 1986.

[42]P. A. Heiney, M. E. Huster, V. B. Cajipe, and J. E. Fisher, Synth. Met. **12**, 21 (1985).

[43]M. E. Huster, Ph.D. thesis, University of Pennsylvania, 1985.

[44]The (00.4) reflection was used instead of the more conventional (00.2) reflection in order to achieve focusing with a reasonable experimental configuration. It was later discovered that this choice resulted in a small amount of $2\lambda/3$ contamination of the beam, which did not quantitatively affect our analysis.

[45]S. Hendricks and E. Teller, J. Chem. Phys. **10**, 147 (1942).

[46]J. Kakinoki and Komura, J. Phys. Soc. Jpn. **7**, 30 (1952); Acta Cryst. **15**, 292 (1962); **19**, 137 (1965).

[47]Note that, in principle, the distribution could be made yet more disordered by incorporating the possibility of "anti-carbon" layers with negative thickness and density, i.e., with

an anti-C layer annihilating the previous C layer. This would have the effect of making the distribution more symmetric, since stage packages with $n < N$ would now be allowed. A similar algorithm has recently been used by P. W. Stephens and A. I. Goldman, Phys. Rev. Lett. **56**, 1168 (1986).

[48]P. A. Heiney, P. W. Stephens, R. J. Birgeneau, P. M. Horn, and D. E. Moncton, Phys. Rev. B **28**, 6416 (1983), and references therein.

[49]Specifically, both the sample and the x-ray beam were very thin and the sample had a somewhat irregular shape, so that the volume of sample illuminated by the beam varied rapidly with scattering angle.

[50]R. Nishitani, K. Suda, and H. Suematsu, J. Phys. Soc. Jpn. **55**, 1601 (1986).

[51]T. F. Rosenbaum, S. E. Nagler, P. M. Horn, and R. Clarke, Phys. Rev. Lett. **50**, 1589 (1984).

[52]E. D. Specht, R. J. Birgenau, K. L. D'Amico, D. E. Moncton, S. E. Nagler, and P. M. Horn, J. Phys. Lett. (Paris) **46**, L561 (1985).

[53]S. E. Nagler, P. M. Horn, T. F. Rosenbaum, R. J. Birgeneau, M. Sutton, S. G. J. Mochrie, D. E. Moncton, and R. Clarke, Phys. Rev. B **32**, 7373 (1985).

[54]R. J. Baxter, J. Phys. **C6**, L445 (1973); R. J. Baxter, H. N. V. Temperley, and S. E. Ashley, Proc. R. Soc. London, Ser. A **358**, 535 (1978).

[55]J. M. Kosterlitz and D. J. Thouless, J. Phys. C **5**, L124 (1972); **6**, 1181 (1973).

[56]R. Clarke, N. Wada, and S. A. Solin, Phys. Rev. Lett. **44**, 1616 (1980).

[57]D. P. DiVincenzo, C. D. Fuerst, and J. E. Fischer, Phys. Rev. B **28**, 1115 (1984).

[58]S. C. Moss, C. Thompson, and H. Zabel, Bull. Am. Phys. Soc. **30**, 240 (1985).

[59]M. J. Winokur and R. Clarke, Phys. Rev. Lett. **56**, 2072 (1986).

[60]F. Rousseaux, R. Moret, D. Guerard, P. Lagrange, and M. Lelaurain, Synth. Met. **12**, 45 (1985).